



Automated detection of male eiders over aerial photographs

Interim Report

Contract #3000682507

Ata Haddadi, Ph.D. & Prof. Brigitte Leblon.
Ph. D.
Phone: (506) 453-4924
Email: bleblon@unb.ca
Fax: (506) 453-3538

Angela Douglas M.Sc.
Executive Director, Coalition-SGSL
Phone:(902) 218-2594
Email: Coalition.sgsl@gmail.com

Mailing Address

University of New Brunswick
Faculty of Forestry and Environmental Management
28 Dinneen Dr
Fredericton, NB
E3B 5A3

1. Background

The current American Common Eider (*Somateria mollissima dresseri*) population estimate is around 300,000 birds and although the distribution and relative abundance of American Common Eider has been well described, there exists no comprehensive monitoring program for the *dresseri* subspecies. Thus, the current challenge is to develop a monitoring program for this population. Several studies have suggested that bird counts based on aerial images may be more accurate and consistent than observer-based counts and as such, we have developed an automated method to count male Common Eiders (COEI_M) over airborne images having a ground pixel size ranging from 3.5 to 4.5 cm.

2. Materials

In 2016, 1200 images were collected with an UltraCam Vexcel Falcon Prime Sensor in Deer Island and Grand Manan Archipelagos in New Brunswick, Canada (Figure 1). The sensor was onboard a plane flying at 477 m altitude. Images were delivered in a geotagged format (geotiff) which included their geolocation. The images were acquired in four bands: blue, green, red, and near-infrared and the ground pixel size range was between 3.5 and 4.5 cm.

Among all 1200 images, the following images acquired in March 24, 2016 and March 30, 2016 were selected: 0080_03242016, 0094_03242016, 0378_03242016, 0570_03242016, 0595_03242016, 0091_03302016, 0092_03302016, 0106_03302016, 0149_03302016, 0150_03302016, 0179_03302016, 0218_03302016, 0242_03302016, 0261_03302016. These images contain the bird species listed in Table 1. They were used to develop the automated detection method for COEI_M.

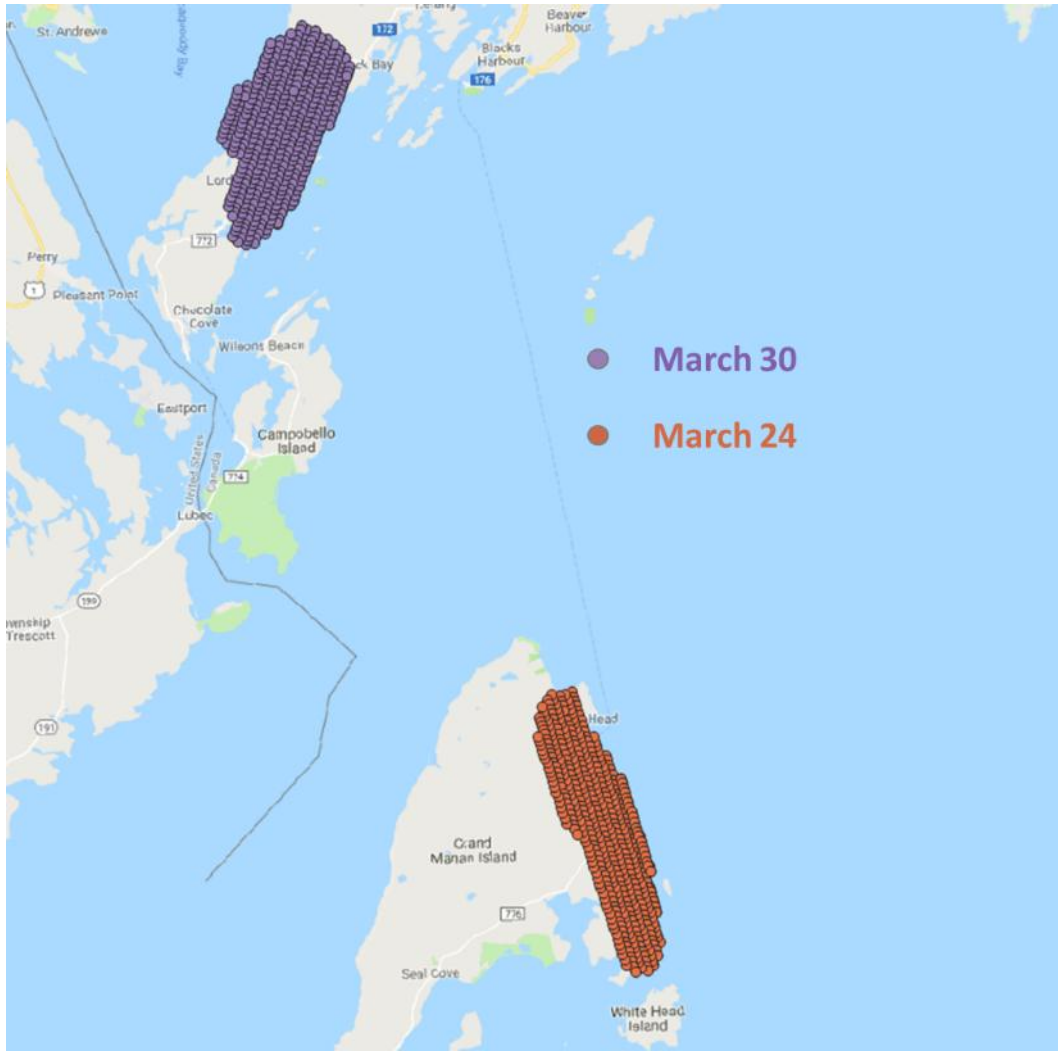








Figure 1. Google Earth image with the location of the images.

Table 1. Bird species located in the images

Code	Name	Latin name	Picture
Brant/ATBR	Flying brant	<i>Branta bernicla</i>	
COEI •COEI_F •COEI_M	Common eider • Male • Female	<i>Somateria mollissima dresseri</i>	
HERG •HERG_S •HERG_F	European herring gull • sitting • flying	<i>Larus argentatus</i>	
LTDU	Long-tailed duck	<i>Clangula hyemalis</i>	
RBME	Red-breasted merganser	<i>Mergus serrator</i>	
GBBG	Great black-backed gull	<i>Larus marinus</i>	

The images also contained buoys, salmon cages, boats, buildings, and small islands (Figure 2). There were buoys in image 0080_03242016, 0378_03242016,

0092_03302016, 0150_03302016, and 0261_03302016. The specular reflection of the waves was obvious in most of the images which increased image noise and in some cases this specular reflection was similar to the bird signature.



Figure 2. Examples of the other objects present in the images such as buoys, salmon cages, boats, buildings, and small islands. The noisy bright spots are due to specular reflection of waves.

3. Methods

In order to locate and categorize the birds as a function of the species, the images were manually photo-interpreted by two bird experts, Dr. Scott Gilliland and Dr. Matthews Mahoney, For each image, a geodatabase file was produced containing the bird location with their species, behavior (flying or sitting), and age (adult or immature). The bird locations that were manually photo-interpreted were used to delineate training areas for the image classifiers as well for validate the classifying method as described. Table 2 gives the number of detected birds in the selected images as a function of their species. In this study, unknown species, UNK, and species with a limited number of birds in the images (GBBG and RBME) were not considered.

Table 2. Number of located birds per species over each image

Image #	Brant	COEI-F	COEI-M	HERG-F	HERG-S	LTDU	GBBG	RBME	UNK**
0080_03242016	29				25				3
0094_03242016				33					
0378_03242016	20	5	10	1					1
0570_03242016				16	39			2	
0595_03242016		30	24	2	3				
0091_03302016				29	102				
0092_03302016				3	25				
0106_03302016		10	7						
0149_03302016				1	17				1
0150_03302016				19	116				
0179_03302016		26	38			30			
0218_03302016		44	57						6
0242_03302016				1	7				5
0261_03302016				24	128		1		
Total	49	115	136	129	462	30	1	2	16

** Unknown species

The aim of this study is to create a method to detect COEI_M. Therefore, the proposed methodology focused only on COEI_M detection. It is presented under a flowchart format in Figure 3. First, the noise and local variation in the image was smoothed with a 2-D convolution filter with a size of 3. This filter decreased the variation in the image based on the averaging of each nine-pixel windows. Chabot et al. (2018) also used a similar approach to decrease the noise in the image. To increase the discrimination between COEI_M and the other objects, including other bird species, algebraic combinations of image bands, called a vegetation index, can be used. The vegetation indices that were used in this study are listed in Table 3. Most of them are common vegetation indices from remote sensing literature. The last one, MEVI, is a modified version of the EVI index that was developed by Huete et al. (1997) for mapping vegetated area MODIS images.

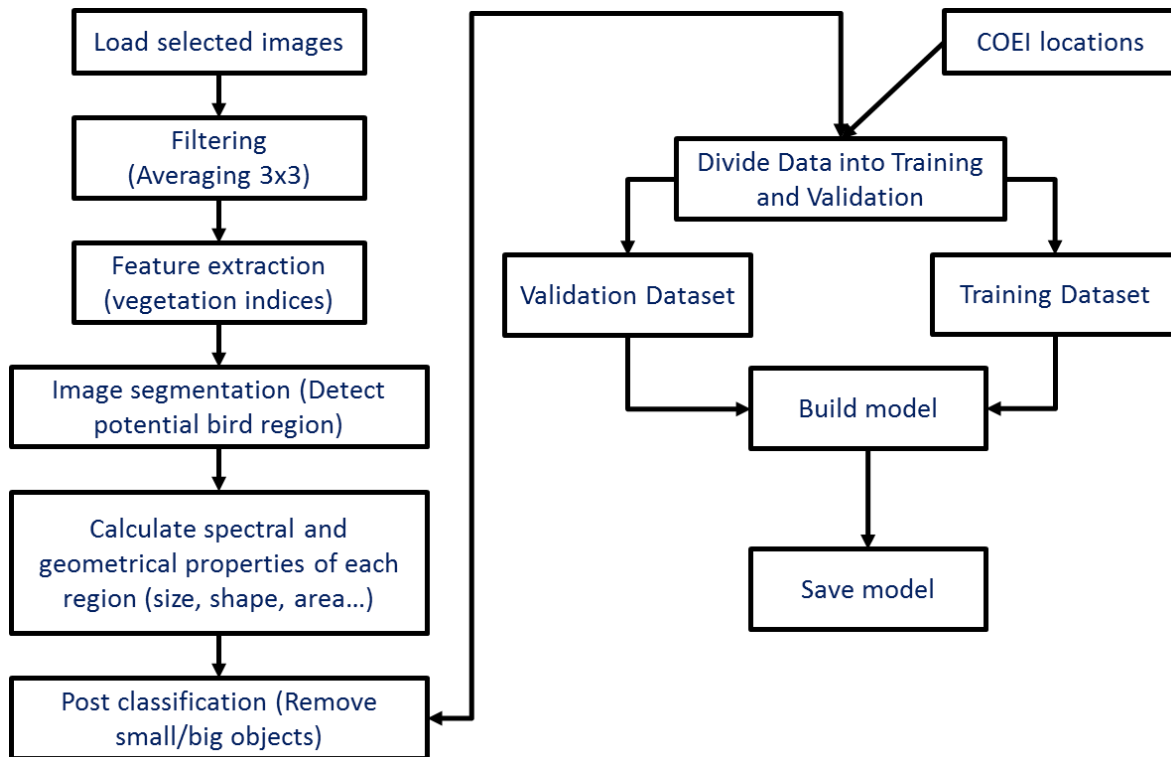


Figure 3 Flowchart of the proposed method to detect COEI_M.
Table 3. Vegetation indices used in the study.

Vegetation Index	Formula	Author	Equation
NDVI	$(NIR-R)/(NIR+R)$	Rouse et al. (1973)	(1)
ExG	$2 \cdot G - B - R$	Meyer and Neto (2008)	(2)
GNDVI	$(NIR-G)/(NIR+G)$	Gitelson et al. (1996)	(3)
VARI	$(G-R) / (B+G+R)$	Gitelson, A., et al. (2002)	(4)
MEVI	$(NIR+G-2 \cdot B)/(NIR+G+2 \cdot B)$	This report	(5)

The image size (11704 x 7920) results in each image having around 93M pixels, so classifying the entire image will be extremely time consuming. There is therefore the need to precisely define potential bird regions and then work to identify the COEI_M birds in these potential regions. For each detected bird region, we computed the spectral signatures (mean and standard deviation of digital numbers associated to each band and each vegetation index) in order to select which band and/or vegetation index was best to detect a bird region. This allowed for masking of the dark sea background and the objects with a different spectral signature. Such masking methods did not require a heavy computation, by contrast to the watershed segmentation method employed by Chabot et

al. (2018) which has the additional disadvantage of leading to over- or under-segmentation depending on the image resolution. However, the mask does not allow for the differentiation of COEI_M birds from the other bird species or objects such as waves that have a similar spectral signature as COEI_M. This is why the following geometrical features were also included in the analysis: area, perimeter, major axis, minor axis, equivalent diameter, solidity, compactness, roundness, form factor, rectangular fit, and elongation. These features are defined in Table 4. Removing the objects that are different than COEI_M is critical in developing a robust method, as outliers have a high impact in the training stage of the classifier.

Table 4. Geometrical features used in this study.

Geometrical features	Description	Reference	Equation
Area (pixel ²)	Total area of the object	Jähne 2005	(6)
Perimeter (pixel)	Total length of the object boundary	Jähne 2005	(7)
Major axis length (pixel)	Major axis length of an ellipse that has the same normalized second central moments as the region.	Jähne 2005	(8)
Minor axis length (pixel)	Minor axis length of an ellipse that has the same normalized second central moments as the region.	Jähne 2005	(9)
Equivalent diameter (pixel)	Circle diameter which has the same area as the region	Jähne 2005	(10)
Solidity (unitless)	Solidity = Area / area of convex hull	Chabot et al., 2018	(11)
Compactness (pixel)	Compactness = $\sqrt{(4 * \text{Area} / \pi) / \text{outer contour length}}$	Chabot et al., 2018	(12)
Roundness (unitless)	Form Factor = $4\pi * \text{Area} / (\text{total perimeter})^2$	Chabot et al., 2018	(13)
Form factor (unitless)	Form Factor = $4\pi * \text{Area} / (\text{total perimeter})^2$	Chabot et al., 2018	(14)
Rectangular Fit (unitless)	Rectangular Fit = Area / (Major Length * Minor Length)	Chabot et al., 2018	(15)
Elongation (unitless)	Elongation = Major Length / Minor Length	Chabot et al., 2018	(16)

To classify the detected objects after masking in two classes (False_COEI_M and True_COEI_M), a classifier was applied to all the bands, vegetation index and all geometrical features. Because of the high number of input features (24), we employed a

Support Vector machine (SVM) classifier as classifier. SVM is one of the best methods for large feature numbers. This algorithm does not require the distribution parameters of the input data (Richards and Jia 2006). Indeed, SVM finds the separating hyperplane based on the pixels that are close to the hyperplane between classes. SVM finds two hyperplanes by:

$$\text{class 1 if } \mathbf{w}\mathbf{x} + w_{n+1} \geq 1 \quad (17)$$

$$\text{class 2 if } \mathbf{w}\mathbf{x} + w_{n+1} \leq -1$$

where \mathbf{x} is the input feature vector, and \mathbf{w} is the weight vector for each hyperplane and N is the number of features. Figure 4 shows the position of hyperplanes and the optimal hyperplane in the case of two classes and two input features.

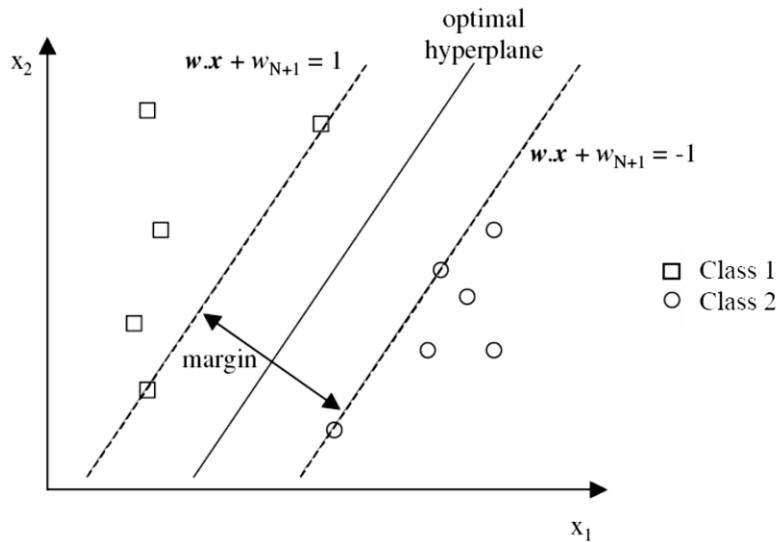


Figure 4. Two hyperplanes to separate class1 and 2 (Richards and Jia 2006).

To find the value of \mathbf{w} , SVM employs a constraint (α) known as a Lagrange Multiplier that minimizes Equation (18) to lead to the maximum allowed margin between classes.

$$L = \frac{1}{2} \|\mathbf{w}\|^2 - \sum \alpha \{y_i(\mathbf{w} \cdot \mathbf{x}_i + w_{n+1}) - 1\} \quad (18)$$

The limited number of COEI_M birds (136) in the images (Table 2) for training and validating the classifier will increase the chance of having a classifier that suffers from overfitting or underfitting. To avoid the problem of overfitting/underfitting in the classification process, the number of objects that are not COEI_M should not be higher

than the COEI_M number (136) and the *k-fold* cross validation approach needs to be used. In this approach, the training dataset is divided into *k* groups. A classification model is built based on *k-1* groups and validated with the group left out. This method is better than one-leave-out cross validation for classification modeling (Bharat Rao et al. 2008). To estimate the absolute performance of the classification method, we also need an independent dataset that should not be used in the training. We selected 20% of the data to validate and calculate the performance of the model. The number of training and validation data for building the classification and validation were 106 and 30, respectively.

4. Results

4.1 Spectral signatures

Figure 5 and Figure 6 compare graphically the bird spectral signature for each band or vegetation index as a function of the species. Figure 6 shows that all bird species have NDVI values between -0.3 and 0.3 and MEVI values of less than 0.2.

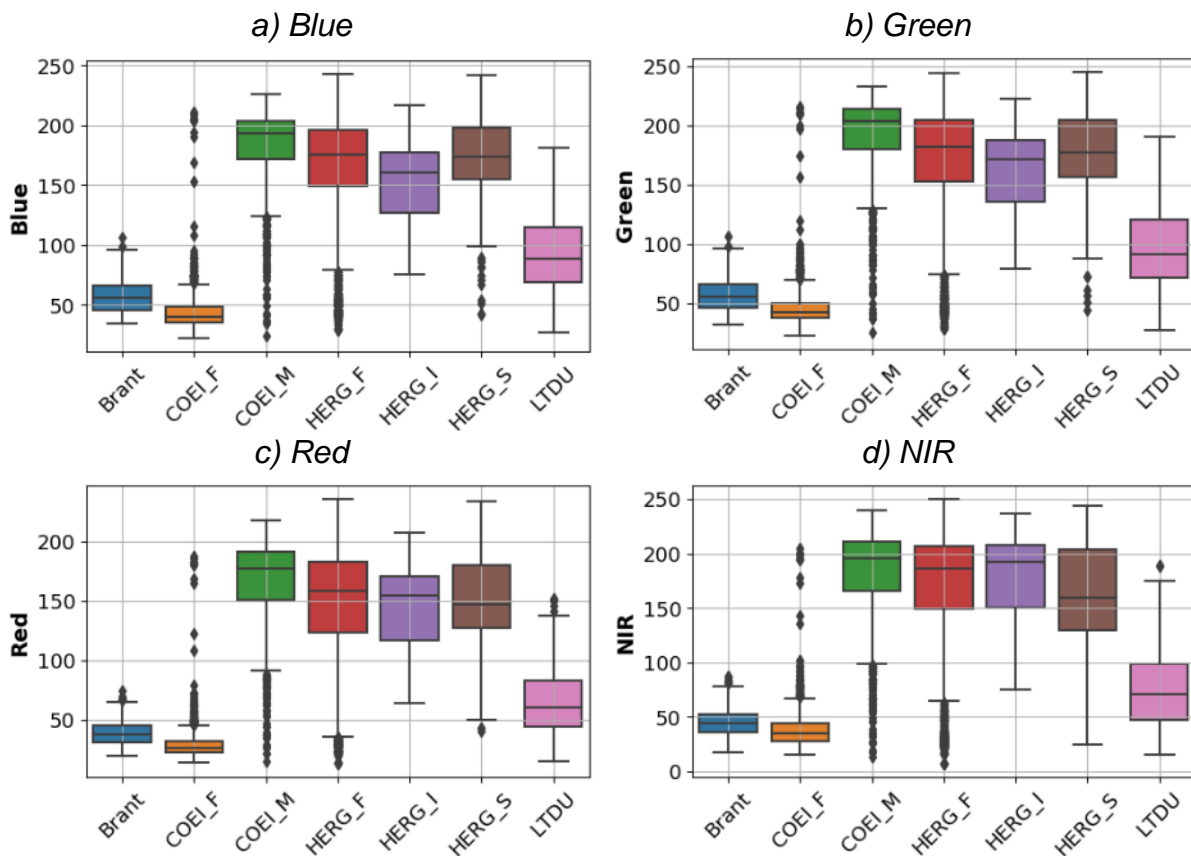


Figure 5. Comparison of the spectral signature of each bird species as a function of the band.

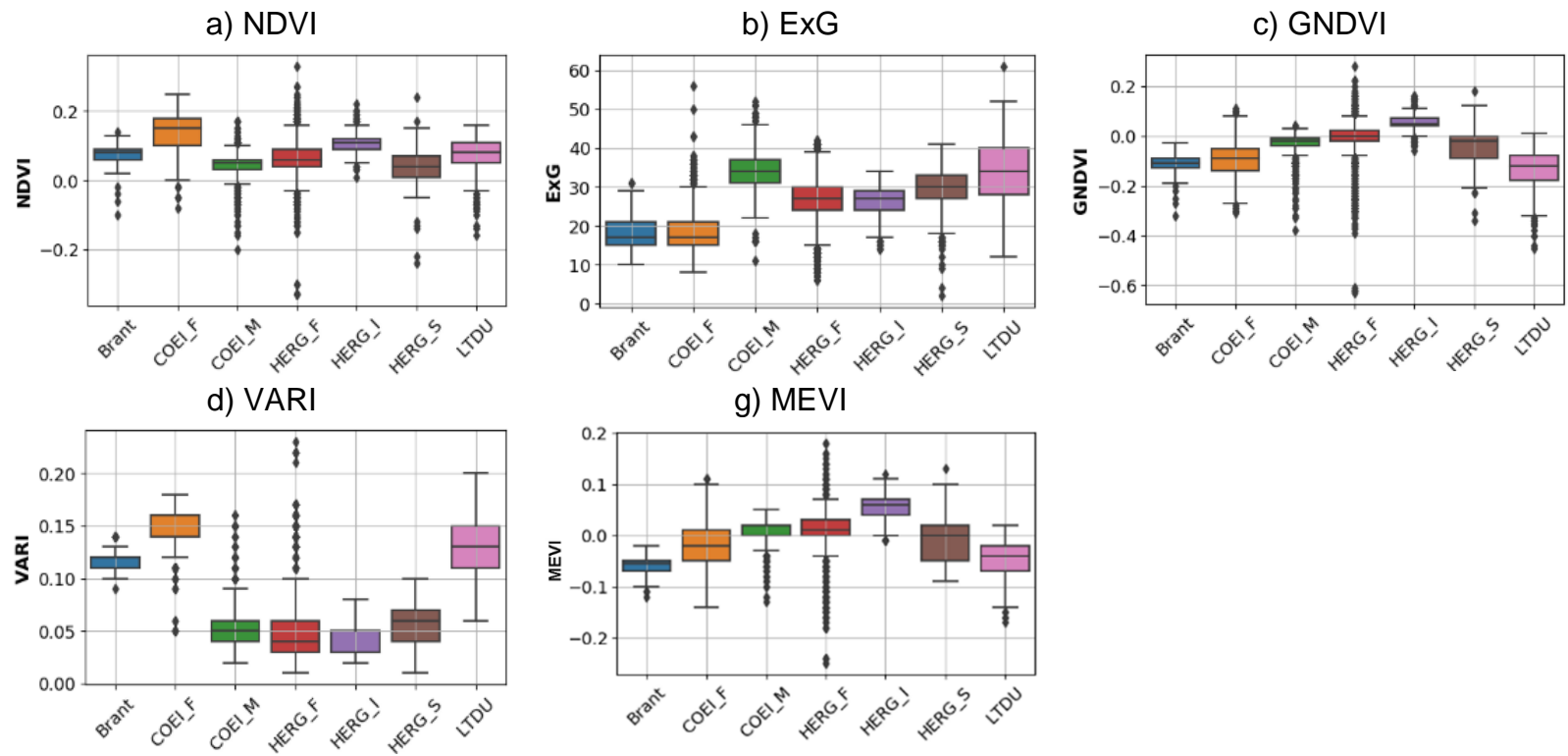


Figure 6. Comparison of the spectral signature of each bird species as a function of the vegetation index.

4.2 Image segmentation

To detect the bird regions, we employed a masking approach based on the MEVI value of less than 0.2 and the NDVI value between -0.3 and +0.3 as defined in the graphical comparison of the spectral signatures. This approach allows removing the dark sea background and objects that are different than birds. Figure 7 shows the potential bird regions for a region of image 0080_03242016 and 0106_03302016. All objects that meet the defined condition for NDVI and MEVI are potential birds. Each bird region is 645cm² which correspond to about 52 pixels given the ground pixel size of 3.5 cm.

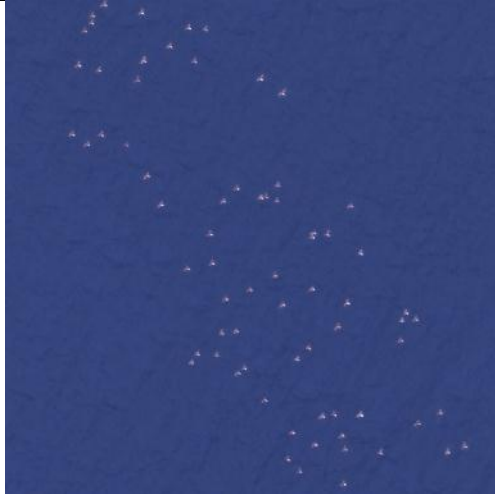
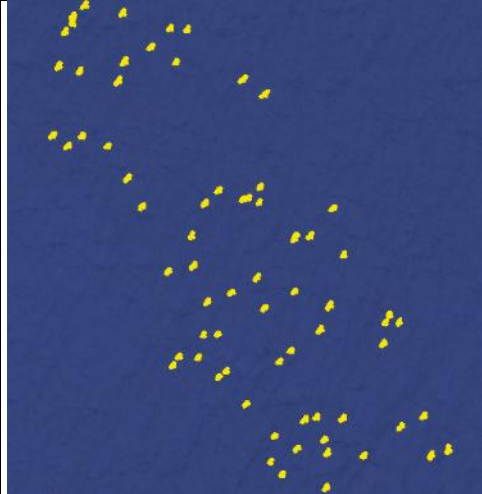

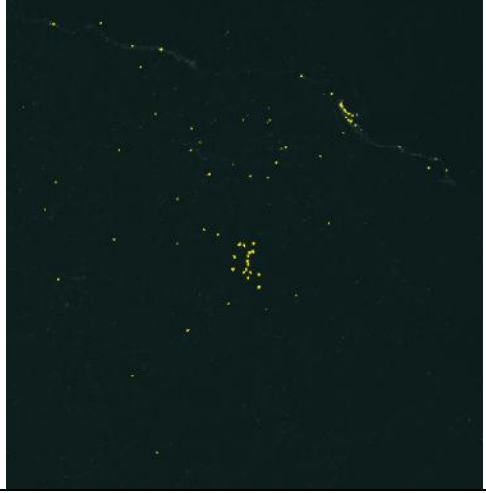
Image #	Before masking	After masking
0080_03242016		
0106_03302016		

Figure 7. Bird regions based on the NDVI-MEVI mask in the case of images 0080_03242016 and 0106_03302016.

4.3 Geometrical features

The image segmentation detects more than 10,000 objects which have the same spectral signatures as the COEI_M birds. However, these objects are geometrically different than the COEI_M birds. Figure 8 compares the true COEI_M and false COEI_M classes with respect to the range of the considered geometrical features. Among all the considered geometrical features, the following ones can be used to characterize the COEI_M class and remove non-bird objects such as waves and bright spots:

- Area range: 15 – 80 pixels
- Perimeter range: 15 – 35 pixels
- Roundness: more than 0.5

Applying these geometrical features decreases the number of objects detected in the previous phase from more than 10,000 to hundreds as objects that are big, small or too different than COEI_M will be removed. A small portion of objects that are to some extent similar to the COEI_M objects will remain.

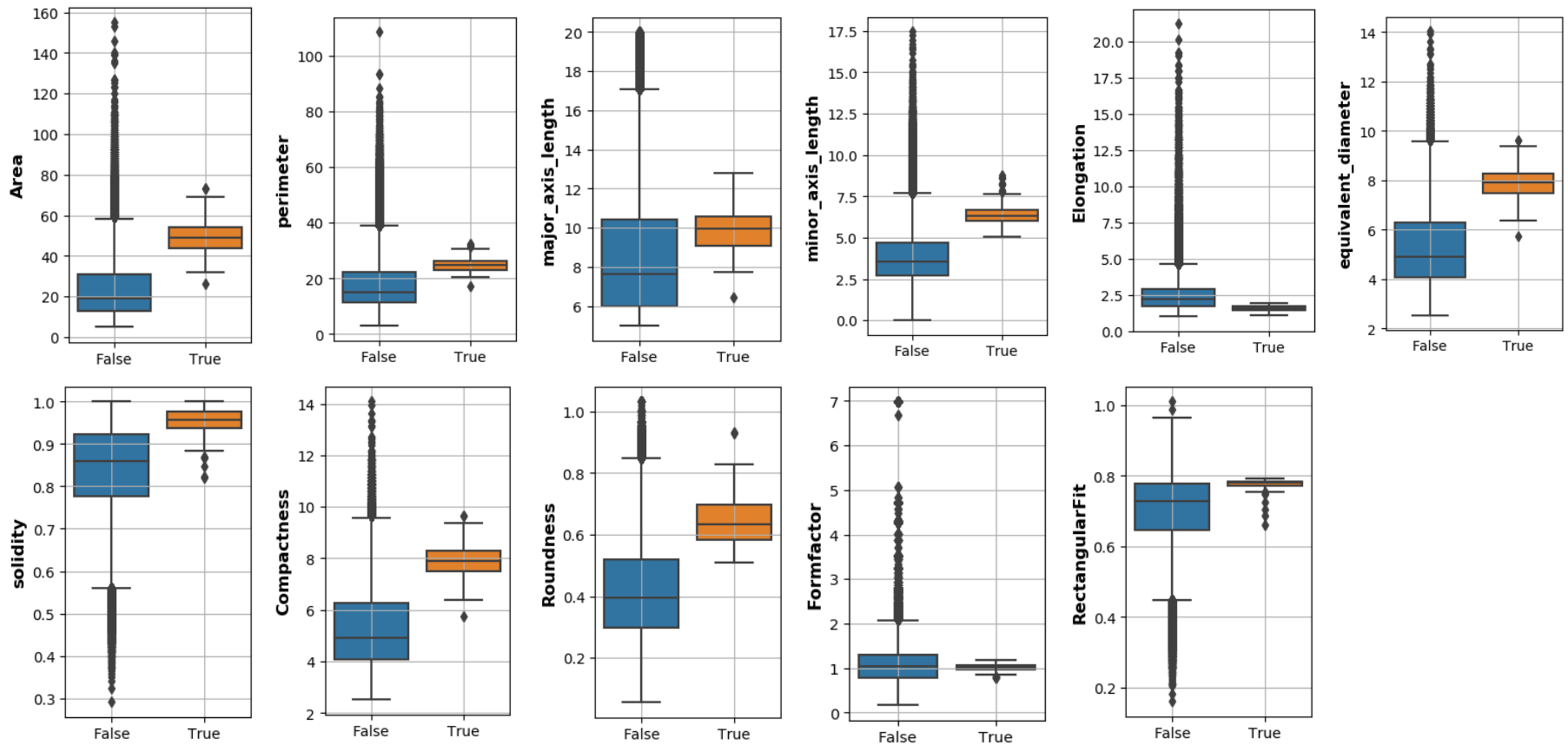


Figure 8. Range of the geometrical variables for the true COEI_M and false COEI_M objects.

4.4 Classification

An SVM classifier was developed to classify the objects into objects that represent COE_M (True) and objects that are not COEI_M (False). Because the number of objects that are not COEI_M is higher than the number of COEI_M, we divided them half for training the classifier (N=552) and for validating it (N=551), while for COEI_M, we kept 20% for the validation dataset (N=30) and the rest for the training dataset (N=106). For all training and validation objects, the spectral and geometrical properties were calculated and an SVM classifier was built. The corresponding confusion matrix is given in Figure 9a for the training dataset and in Figure 9b for the validation dataset.

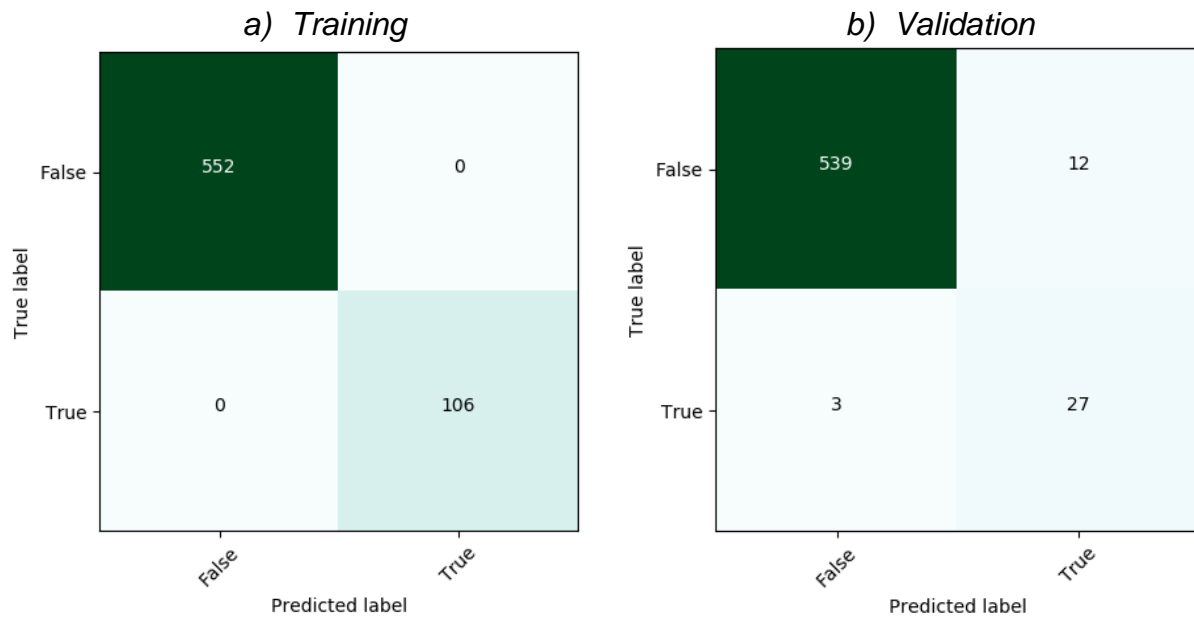


Figure 9. Confusion matrix (in number of objects) for the SVM classifier into two classes (True COEI_M and False COEI_M) in for a) the training dataset and b) the validation dataset.

The overall classification accuracy is 100% with the training dataset and 97% with the validation dataset. In the validation dataset, 10% of the 30 objects (i.e., 3 objects) that are true COEI_M were classified as False COEI_M objects, which means that the accuracy of the true COEI_M class is 90%. 12 over 551 False COEI_M objects were classified which means that the accuracy of the false COEI_M class is 98%. Table 5 gives the comparison between the number of COEI_M manually identified and the number of

COEI_M automatically identified as a function of the image number and the image pixel size.

Table 5. Comparison between the number of COEI_M birds manually identified and the number of COEI_M birds automatically identified as a function of the image number. The image pixel size is also given.

Image #	Proposed method	Manually	Pixel Size (cm)
0080_03242016	0	0	3.79
0094_03242016	0	0	3.88
0378_03242016	11	10	3.92
0570_03242016	0	0	3.78
0595_03242016	25	24	3.81
0091_03302016	2	0	3.67
0092_03302016	2	0	3.66
0106_03302016	9	7	3.67
0149_03302016	0	0	3.67
0150_03302016	0	0	3.64
0161_03302016	0	0	3.80
0179_03302016	37	38	3.68
0218_03302016	57	57	3.78
0242_03302016	0	0	3.86
0261_03302016	1	0	3.85

Most images were processed with good accuracy. For some images where there were only one or two COEI_M birds, the method did not detect any birds. The detection accuracy does not appear to be related to the image pixel size. However, the method was tested over a limited number of images containing COEI_M birds and needs to be tested on more images. In Figure 10, the detected COEI_M birds are displayed for two different regions of three images. In Region 2 image #0378_03242016 the proposed method could detect one COEI_M which was not digitized manually. In Region 1 of image #0179_03302016, all COEI_M birds were detected. The reason for this false classification is that the COEI_M bird shape is much different than other COEI_M.


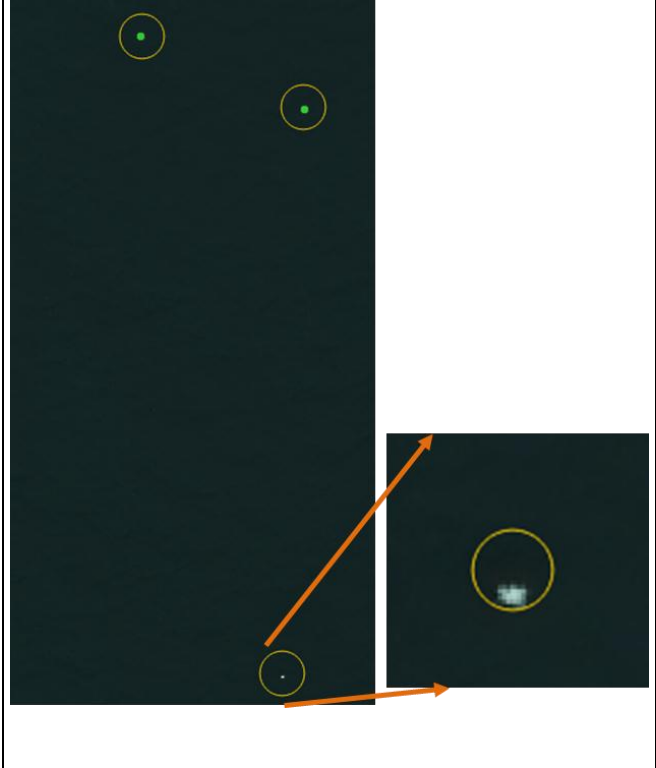
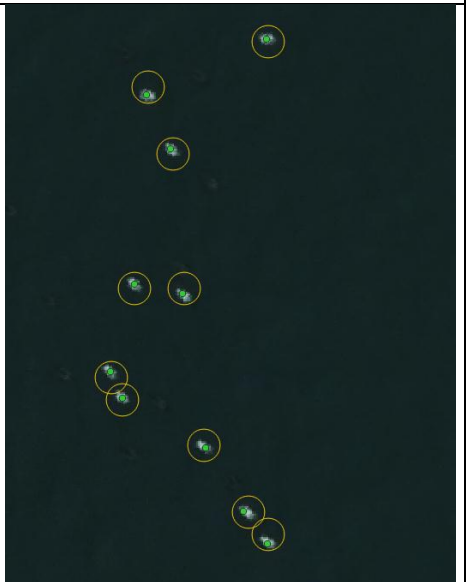
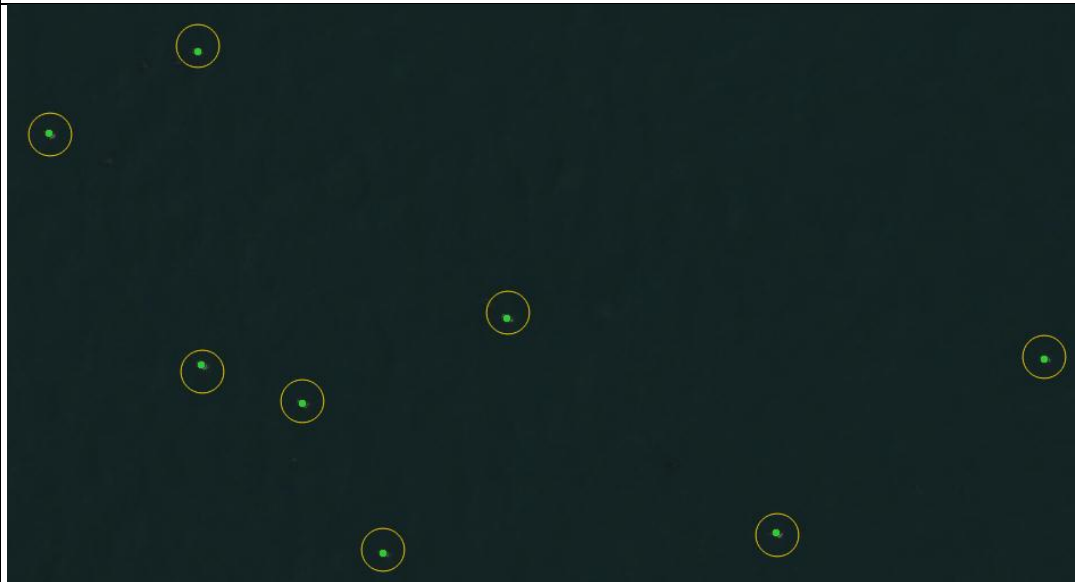
Image #	Region 1	Region 2
0378_03242016		

Image #	Region 1	Region 2
0595_03242016		

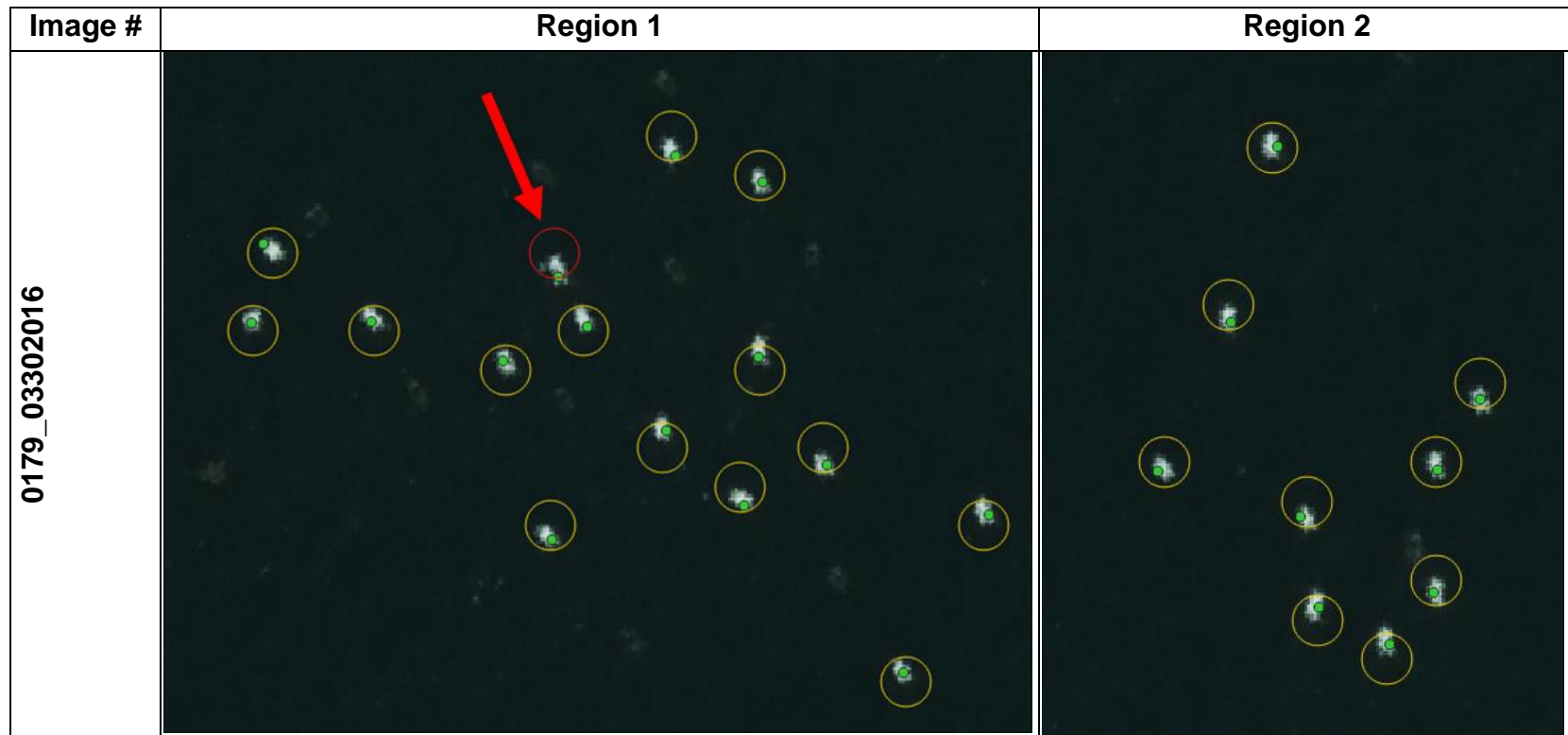


Figure 10. Identified COEI_M birds in some images based on the purposed method. The green dots are the digitized COEI_M manually and the yellow round shapes are COEI_M derived from the purposed method. The red round shape is the false classified from our method.

5. Conclusions

This study proposes an automated method to detect male Common Eiders (COEI_M) *Somateria mollissima dresseri* over airborne images having a ground pixel size ranging from 3.5 to 4.5 cm. The images were acquired in the blue, green, red, and near-infrared bands. Potential bird regions (objects) were delineated by masking out the dark sea background and other features that have a different spectral signature based on NDVI and MEVI threshold values. For each object, the spectral signatures and various geometrical features were calculated to obtain a total of 24 input features for the classifier. Small and large objects were removed based on thresholds for three geometrical properties (area, perimeter, roundness). A training and validation dataset were created with all the remained bird objects detected over all the images. Then a support vector machine classifier with a cross-validation approach was applied to both the training and validation datasets to classify the objects into the true and false COEI_M classes. The overall classification accuracy was 100% with the training dataset and 98% with the validation dataset. In the validation dataset, only 10% of the true COEI_M objects were classified as false COEI_M leading to an accuracy of 90%. The classifier was applied to all the images and the resulting detected number of birds matched closely the numbers resulting from the manual photo-interpretation of the images. The proposed method has been developed over a rather small sample and needs to be tested over a large database.

6. Acknowledgments

The authors thank Dr. Scott Gilliland and Dr. Matthews Mahoney for their photointerpretation and providing the data for this project. The study was funded by a contract from Environment and Climate Change Canada awarded to the Southern Gulf of St. Lawrence Coalition on Sustainability.

7. References

Bharat Rao, R., Fung, G., Rosales R. (2008) On the dangers of cross-validation. An experimental evaluation, Proceedings of the SIAM International Conference on Data Mining, SDM 2008, April 24-26, 2008, Atlanta, Georgia, USA, pp. 588-596.

Chabot, D., Dillon, C., Francis, C.M. (2018) An approach for using off-the-shelf object-based image analysis software to detect and count birds in large volumes of aerial imagery. *Avian Conservation and Ecology* 13(1) :15, doi: 10.5751/ACE-01205-130115

Gitelson, A.A., Kaufman, Y.J., Merzlyak, M.N. (1996) Use of a green channel in remote sensing of global vegetation from EOS-MODIS. *Remote Sensing of Environment* 58, 289–298

Gitelson, A.A., Kaufman, Y.J., Stark, R., Rundquist, D. (2002) Novel algorithms for remote estimation of vegetation fraction, *Remote Sensing of Environment* 80, 76-87

Huete, AR, Liu, HQ, Batchily, K, van Leeuwen, W (1997) A comparison of vegetation indices over a global set of TM images for EOS-MODIS. *Remote Sensing of Environment* 59(3): 440-451. doi: 10.1016/S0034-4257(96)00112-5.

Jähne, B. (2005) *Digital Image Processing*. Springer-Verlag, Berlin-Heidelberg, 6th edition, p. 608

Meyer, G., Neto, C. (2008) Verification of color vegetation indices for automated crop imaging applications, *J Comput. Electron. Agric.*, 63:2, 282-293, doi: 10.1016/j.compag.2008.03.009

Richards JA, Jia X (2006) *Remote sensing digital image analysis: An introduction*. Springer, Berlin, Germany, p. 420

Rouse, J.W., Haas, R.H., Schell, J.A., Deering D.W. (1973) Monitoring vegetation systems in the Great Plains with ERTS. In *Proceedings of the Third ERTS Symposium*, NASA: Washington, DC, USA, 10–14 December 1973 NASA SP-351, pp. 309–317